Journal of Power Sources 395 (2018) 251–261

Contents lists available at ScienceDirect

Journal of Power Sources

journal homepage: www.elsevier.com/locate/jpowsour

A look into the voltage plateau signal for detection and quantification of lithium plating in lithium-ion cells

Xiao-Guang Yang, Shanhai Ge, Teng Liu, Yongjun Leng, Chao-Yang Wang*

Department of Mechanical and Nuclear Engineering and Electrochemical Engine Center (ECEC), The Pennsylvania State University, University Park, PA 16802, USA

HIGHLIGHTS

- We present a Li-ion battery model incorporating both Li plating and stripping.
- Voltage plateau after charging due to by Li stripping is captured and analyzed.
- Length of voltage plateau depends highly on capability of graphite intercalation.
- Anode splits into to two parts during Li stripping.
- Differential voltage approach to quantify Li plating amount is assessed.

GRAPHICAL ABSTRACT

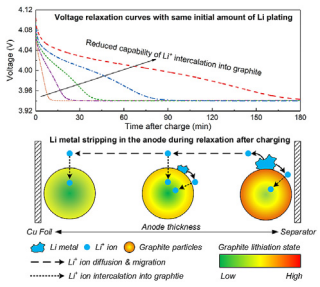

ARTICLE INFO

Keywords:
Lithium-ion battery
Lithium plating
Lithium stripping
Voltage plateau
Graphite anode
Electrochemical modeling

ABSTRACT

Voltage plateau during relaxation or discharge after charging is a distinct signal associated with stripping of deposited Li metal and hence a feasible tool for online detection of Li plating in Li-ion batteries. Here, we present a physics-based model with incorporation of Li plating and stripping to gain a fundamental understanding of the voltage plateau behavior. Specifically, we focus on the internal cell characteristics when voltage plateau occurs and on key factors affecting the shape and duration of voltage plateau. Furthermore, the validity of using the duration of voltage plateau for estimating Li plating amount is assessed. It is found that the duration of voltage plateau depends on the rate of Li stripping, while the stripping rate is restricted by the capability of Li^+ intercalation into graphite. Parameters like intercalation kinetics, solid-state diffusivity of graphite and cell temperature can substantially influence the voltage curves even with the same amount of Li plating. Further, we report an interesting phenomenon that during Li stripping one part of anode near the separator has net oxidation current (local stripping rate > intercalation rate), providing Li^+ ions and electrons to the other part of anode near the foil which has net reduction current.

1. Introduction

The last decade has witnessed an unprecedented penetration of Li-ion batteries (LiBs) into the market in various applications like electric vehicles and energy storage systems. These applications require LiBs to be of great durability and safety [1-6]. Carbon-based materials, in particular, graphite, are utilized as anode materials in most state-of-the-art LiBs. A critical challenge to the use of graphite anode is metallic Li deposition, also known as Li plating, which can induce drastic capacity loss as well as safety hazards [7-11]. Detection of Li plating is therefore crucial, especially for real-world applications.

Today's methods for detection of Li plating can be divided into the following categories: a) *Measurement of anode potential vs Li/Li$^+$ with a reference electrode* [12-15]. A general criterion is that Li plating occurs

* Corresponding author.
E-mail address: cxw31@psu.edu (C.-Y. Wang).

https://doi.org/10.1016/j.jpowsour.2018.05.073
Received 1 April 2018; Received in revised form 25 April 2018; Accepted 22 May 2018

at anode potential < 0 V. b) *Post-mortem imaging of anode morphology* [16, 17]. c) *Electron paramagnetic resonance* [18, 19] *and nuclear magnetic resonance* [20, 21] to detect a particular range of resonance frequency corresponding to metallic Li. d) *High precision measurement of coulombic efficiency* [22, 23]. Dahn's group [22] proposes that the plots of coulombic inefficiency per hour versus time fall on the same curve for different tests if cell aging is dominated by solid electrolyte interphase (SEI) growth. Deviation from this curve indicates Li plating. e) *Measurement of cell thickness* [24-27]. Li metal deposition is revealed to induce larger volume change than Li^+ intercalation into graphite, estimated to be 0.37 cm^3/Ah [24]. It is also reported that thickness change becomes irreversible when Li plating occurs. f) *Measurement of graphite lithiation degree via in-situ neutron diffraction* [28]. Zinth et al. [28] found that the lithiation degree of graphite increased by 17% in the relaxation process after C/5 charge at -20 °C, indicating that at least 17% of Li was plated in the charging process. g) *Detection of a distinct voltage plateau after charging* [29-36]. The voltage plateau is ascribed to stripping of deposited Li metal and thus indicates that Li is plated during charging. The voltage plateau can occur either at the beginning of discharge [29-31] or of relaxation [32-36] after charging. A brief summary of the above works are given in Table 1.

Among the above methods, voltage plateau is the most feasible method for online detection of Li plating in real-world applications, as it is nondestructive and does not require special and expensive equipment. Smart et al. [29, 30] were among the first to apply discharge voltage plateau after low temperature (-40 °C) charging as a tool for Li plating detection. They also proposed that the length of plateau can be used as a metric for evaluating Li metal amount. Petzl and Danzer [31] presented a differential voltage approach to detect and quantify Li plating. In their tests, a cell was charged with 1C rate at < -20 °C and discharged immediately after charging. A voltage plateau appeared at the beginning of discharge. Plotting the derivative of voltage over capacity (dV/dQ), they found a distinct dV/dQ peak at the beginning of discharge. They proposed that this dV/dQ peak indicates the end of Li metal stripping, and the discharge capacity at the dV/dQ peak corresponds to the total amount of Li plated during charging. Later, Uhmann et al. [32] proposed to detect voltage plateau during relaxation rather than during discharge, which is advantageous as the cell has no net current at open-circuit, making the plateau more pronounced and easier to detect. This method was then adopted by many other researchers [33-36]. Schindler et al. [33] extended their differential voltage approach to the relaxation process by plotting the derivative of voltage over time (dV/dt), and found a similar peak in dV/dt curve attributed to Li stripping. Bauer et al. [34] applied a similar method to study the impacts of charging temperature on Li plating and found that the duration of voltage plateau was longer at lower charging temperatures. This work is more close to real-world applications as the tested cell is a commercial large-size (16Ah) cell and the testing temperature is more practical (-7.5 °C ~ +27.5 °C, other than extreme cold temperature in the past). Luders et al. [35] further applied the voltage relaxation method along with in-situ neutron diffraction to examine the impacts of charge rate on Li plating, with a 1.95Ah 18650 cell charged at -2 °C. A very interesting finding is that the increase of Li plating amount, estimated by the gain in graphite lithiation degree during cell relaxation measured by neutron diffraction, is proportional to the increase of the duration of voltage relaxation plateau, estimated by the time to reach the dV/dt peak. These results indicate that the time to reach dV/dt peak can be used for assessing the Li plating amount in different tests.

Overall, the prior work demonstrated the feasibility of adopting voltage plateau as a method for Li plating detection. Despite the significant progress in the past several years, there is still lack of fundamental understanding of the voltage plateau behavior. For instance, it is known that the distinct voltage plateau is ascribed to Li metal stripping, but how fast can Li metal be stripped? What factors affect the rate of Li stripping? Which factor is the rate-limiting step? Further, either the discharge capacity at dV/dQ peak or the time to reach dV/dt peak has been proposed as metrics for comparing Li plating amount. Are these methods valid under most circumstances? The objective of the present work is to answer the above questions by a fundamental study of the voltage plateau behavior with the help of mathematical modeling.

Mathematical models have been extensively applied to predict performance and life of LiBs and gain fundamental insights into the internal cell characteristics.[37-44] Several works have been reported to study Li plating during overcharge [45, 46] or during charge at high rates and/or low temperatures [21, 47], and to study the capacity loss induced by Li plating [48]. These models, however, only considered Li plating process and neglected Li stripping process; thus cannot capture the voltage plateau behavior. To the best of our knowledge, only the work of Hein and Latz [49] in the literature ever attempted to simulate Li stripping and the associated voltage plateau behavior, using a 3D microscopic model. It is shown that Li metal distribution is highly non-uniform in the anode. The predicted voltage plateau in this work, however, only lasts a few seconds, rather than tens of minutes as reported in experimental studies.

Here, we present a mathematical model incorporating both Li plating and stripping and apply it to study the voltage plateau behavior after charging at low temperatures. Both the plateau during relaxation and that during discharge are studied. We also perform experiments to validate the model in terms of voltage curves during charge, relaxation, and discharge. The main objectives are to gain fundamental insight into

Table 1
A brief summary of literature work on Li plating detection and quantification

Methods	Description of physics/criteria for Li plating detection	Refs
Three-electrode diagnostics	• Li plating occurs at anode potential < 0V.	[12-15]
Electron paramagnetic resonance (EPR)	• The EPR signal of Li metal is much narrower and its signal center is slightly upfield compared with the EPR signal of Li_xC_6. • The magnitude of EPR signal is related to Li metal amount.	[18, 19]
^{7}Li Nuclear magnetic resonance (NMR)	• The chemical shift of Li metal in NMR spectra (245–270 ppm, depending on Li metal structure) is markedly different from the chemical shift of Li in graphite (~40 ppm). • The peak intensity in NMR spectra is proportional to Li amount and is used to quantify Li plating.	[20, 21]
Measurement of coulombic efficiency (CE)	• If SEI growth is the only aging mechanism, plots of coulombic inefficiency (1-CE) per hour versus time shall fall on the same curve regardless of charge rate. Li plating leads to additional capacity loss and hence to deviation from this curve.	[22, 23]
Measurement of cell thickness	• For the same amount of charge (e.g. 1Ah), the volume change of Li metal is 0.49 cm^3, much larger than graphite (0.12 cm^2). Hence, Li plating leads to a larger increase in cell thickness than Li^+ intercalation.	[24-27, 34]
In-situ neutron diffraction	• The intensity of neutron diffraction data is used to calculate graphite lithiation degree. The increase of graphite lithiation degree in the relaxation process after charging indicates the amount of Li stripped.	[28, 35]
Detection of voltage plateau	• The mixed potential associated with simultaneous Li stripping and Li^+ intercalation leads to a voltage plateau.	[29-36]

the internal cell characteristics when voltage plateau occurs and to explore key factors affecting the voltage curves during Li stripping.

2. Model description

The model in this work is based on our previous electrochemical-thermal (ECT) model [37-41] with modifications to incorporate Li plating and stripping. The ECT model solves the following governing equations:

Charge conservation in the solid electrodes:

$$\nabla\cdot(\sigma_s^{eff}\nabla\phi_s) = j_{tot} \tag{1}$$

Charge conservation in the electrolyte:

$$\nabla\cdot(\kappa_e^{eff}\nabla\phi_e) + \nabla\cdot(\kappa_D^{eff}\nabla\ln c_e) = -j_{tot} \tag{2}$$

Species conservation in the electrolyte:

$$\frac{\partial(\varepsilon c_e)}{\partial t} = \nabla\cdot(D_e^{eff}\nabla c_e) + \frac{1-t_+}{F}j_{tot} \tag{3}$$

Species conservation in the active material particles:

$$\frac{\partial c_s}{\partial t} = \frac{1}{r^2}\frac{\partial}{\partial r}\left(D_s r^2\frac{\partial c_s}{\partial r}\right) \tag{4}$$

Energy conservation of the whole cell (lumped thermal model):

$$mc_p\frac{dT}{dt} = Q + hA(T_\infty - T) \tag{5}$$

Details of the governing equations can be found in the literature [37-41] and are not repeated here. Only the modifications made to account for Li plating and stripping are detailed below.

A major difference of this model with previous Li plating models is the consideration of Li stripping. The reaction of Li metal (Eq. (6a)) is considered reversible and occurs in parallel with the reaction of Li^+ intercalation/de-intercalation of graphite (Eq. (6b)) in the anode:

$$Li^+ + e^- \underset{Stripping}{\overset{Plating}{\rightleftarrows}} Li(s) \tag{6a}$$

$$C_6 + Li^+ + e^- \underset{Deintercalation}{\overset{Intercalation}{\rightleftarrows}} LiC_6 \tag{6b}$$

It is worth mentioning that a portion of Li metal can react with electrolyte to form new SEI layer, as reported by Wandt et al. [19], and the SEI layer of graphite particles also grows with time; both can lead to irreversible Li inventory loss. Nevertheless, as the present work focuses only on one charge-discharge cycle at a low temperature of 0 °C, the rate of SEI formation and growth would be minimal compared with the rates of Li^+ intercalation and Li plating. As such, the parasitic reaction of SEI formation and growth is neglected in this work. The total current density of the anode (j_{tot} in Eqs. (1)–(3)) is the sum of the current density of the above two individual reactions, as:

$$j_{tot} = j_{gr} + j_{Li} \tag{7}$$

where j_{gr} and j_{Li} are current densities of graphite and of Li metal respectively. The current density of graphite is calculated by the following Bultler-Volmer equation:

$$j_{gr} = ai_{0,gr}\left(\exp\left(\frac{\alpha_{a,gr}F}{RT}\eta_{gr}\right) - \exp\left(-\frac{\alpha_{c,gr}F}{RT}\eta_{gr}\right)\right) \tag{8}$$

where gr denotes graphite, a the specific surface area, i_0 the exchange current density, α_a and α_c the anodic and cathodic charge transfer coefficients and η the overpotential. The exchange current density of graphite is calculated as:

$$i_{0,gr} = k_{gr}c_{s,i}^{\alpha_{c,gr}}\cdot c_e^{\alpha_{a,gr}}(c_{s,\max} - c_{s,i})^{\alpha_{a,gr}} \tag{9}$$

where k_{gr} is a rate constant depending on temperature, $c_{s,i}$ the Li^+ ion concentration at graphite surface, c_e the electrolyte concentration and $c_{s,max}$ the maximum Li^+ concentration of graphite.

As Li metal reaction is considered reversible, Butler-Volmer equation is used to calculate the current density instead of the Tafel equation in previous works. Here, we employ the following form of Butler-Volmer equation proposed by Chen et al. [50] for modeling of Li deposition and stripping in Li metal batteries, which is similar to the work of Chadwick et al. [51] for modeling of magnesium deposition and dissolution:

$$j_{Li} = ai_{0,Li}\left(\frac{c_{Li}}{c_{Li}^*}\exp\left(\frac{\alpha_{a,Li}F}{RT}\eta_{Li}\right) - \frac{c_e}{c_e^*}\exp\left(-\frac{\alpha_{c,Li}F}{RT}\eta_{Li}\right)\right) \tag{10}$$

where c_{Li} is the concentration of Li metal, which is calculated based on the Faraday's law:

$$\frac{\partial c_{Li}}{\partial t} = -\frac{j_{Li}}{F} \tag{11}$$

The terms c_{Li}^* and c_e^* in Eq. (10) are reference concentrations of Li metal and electrolyte, based on which the exchange current density $i_{0,Li}$ is defined, as [50]:

$$i_{0,Li} = Fk_{0,Li}(c_{Li}^*)^{\alpha_{c,Li}}(c_e^*)^{\alpha_{a,Li}} \tag{12}$$

where $k_{0,Li}$ is a rate constant. It should be mentioned that the value of $i_{0,Li}$ reported in the literature varied by two orders of magnitude [45]. In this work, c_e^* is set to be the initial lithium salt concentration of electrolyte (1 mol/L), and c_{Li}^* and $k_{0,Li}$ are treated as fitting parameters. Other electrochemical kinetic parameters related to the above two reactions are adopted from the work of Arora et al [45], as summarized in

Table 2
Cell design information and electrochemical kinetic parameters

Cell design information			
Parameter	Anode (Graphite)	Separator	Cathode (NMC622)
Thickness (μm)	48.7	25	40.75
Porosity	0.32	0.4	0.33
Loading (mAh/cm^2)	2.0	/	1.85
Electrolyte (lithium salt) concentration (mol/L)	/	1.0	/
Particle radius (μm)	10	/	5

Electrochemical kinetic parameters		
Parameter	Graphite intercalation/de-intercalation	Li metal plating/stripping
Exchange current density, i_0 (mA/cm^2)	0.21 [45]	5.0 [ad]
Anodic charge transfer coefficient, α_a	0.5 [45]	0.3 [45]
Cathodic charge transfer coefficient, α_c	0.5 [45]	0.7 [45]

[ad] Adjusted, reported values in the literature vary by two orders of magnitude

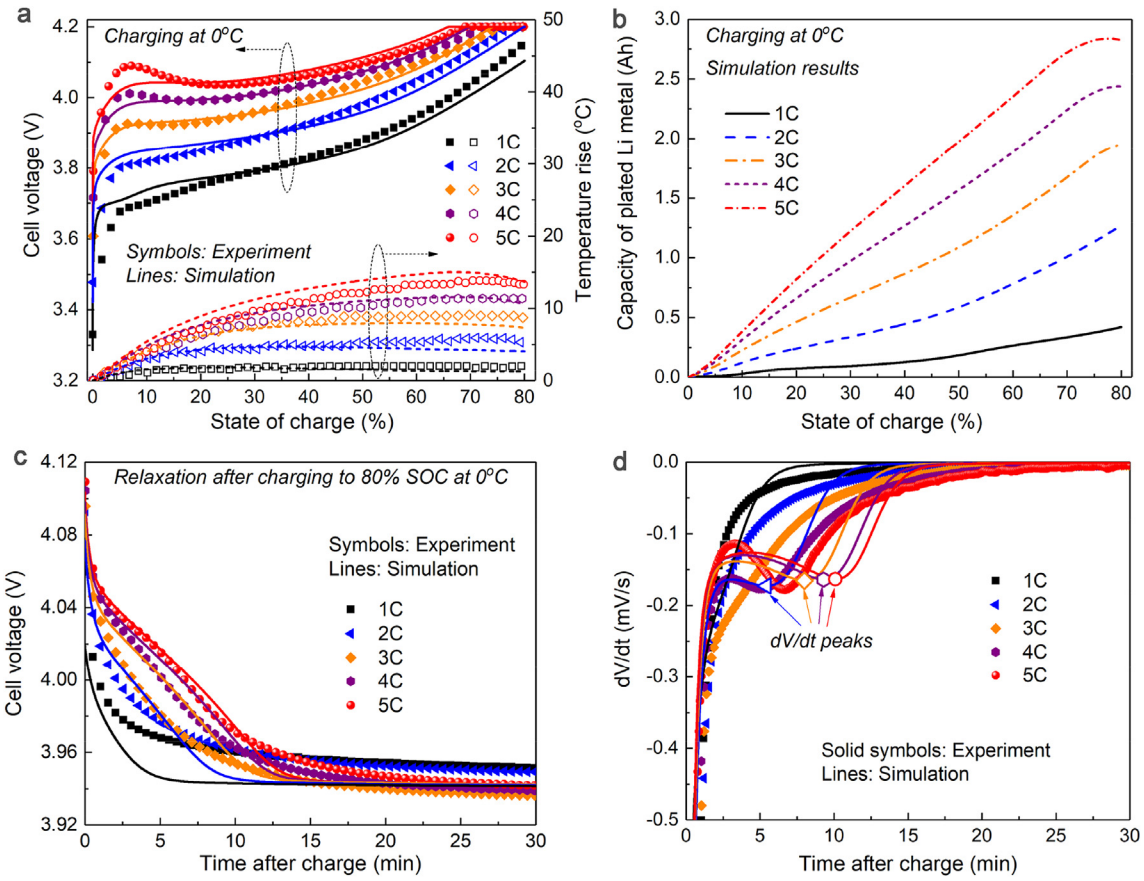

Fig. 1. Model validation and effect of charge rate on voltage relaxation curves. (a) Model and experiment results in terms of voltage and temperature curves during charging with different C-rates. The cell was charged at 0 °C from 0% to 80% state of charge (SOC). (b) Model-predicted Li plating amount vs SOC during charging. (c) Voltage curves during the relaxation process after charging. (d) Differential voltage over time (dV/dt) in the relaxation process after charging.

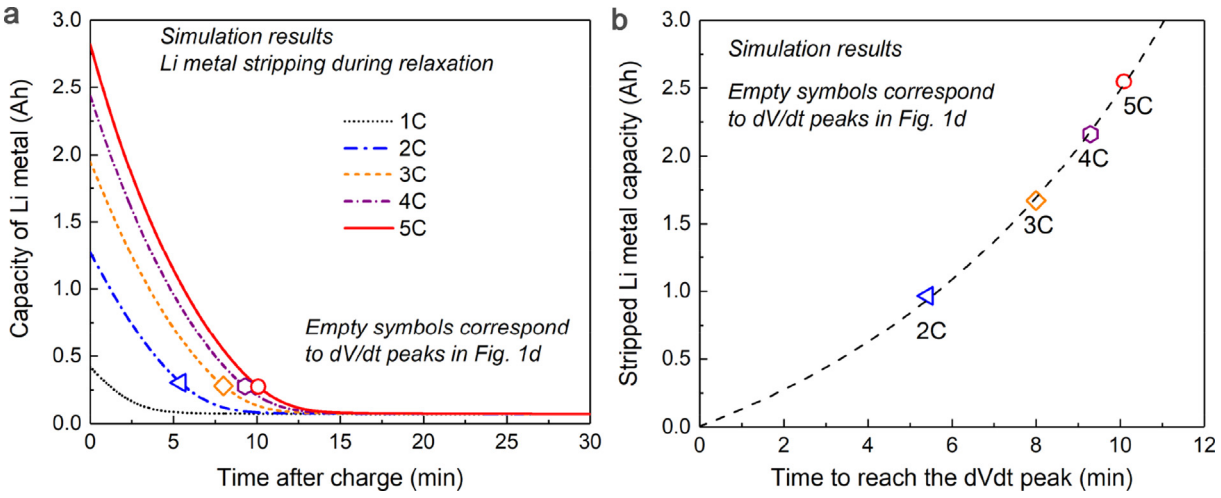

Fig. 2. Analysis of the dV/dt peak. (a) Total remaining Li metal capacity in the cell vs time in the relaxation process predicted by the model. (b) Total amount of Li metal stripped when reaching the dV/dt peak vs the time to reach the dV/dt peak.

Table 2. It is worth mentioning that the introduction of the term c_{Li}/c_{Li}^{*} prior to the first exponential term in Eq. (10) is essential for modeling of Li stripping when Li metal concentration becomes quite low. If this term is neglected as in Refs. [21, 46], Eq. (10) would produce unreasonably high oxidation (Li stripping) current at large positive overpotential (η_{Li}) even when there is no Li metal ($c_{Li} \approx 0$) in the anode.

3. Experiment

A Li-ion pouch cell fabricated by EC Power, LLC, USA, for plug-in hybrid EV application is tested in this work. The cell employs graphite as anode, $LiNi_{0.6}Mn_{0.2}Co_{0.2}O_2$ (NMC622) as cathode, and 1 mol/L $LiPF_6$ in EC/EMC (3:7 by wt.) + 2wt% VC as electrolyte. The cathode was prepared by coating NMP-based slurry onto 15 μm thick aluminum foil, whose dry material consisted of NMC622 (91.5 wt%), Super-C65 (4.4 wt%) and PVdF (4.1 wt%). The anodes were prepared by coating

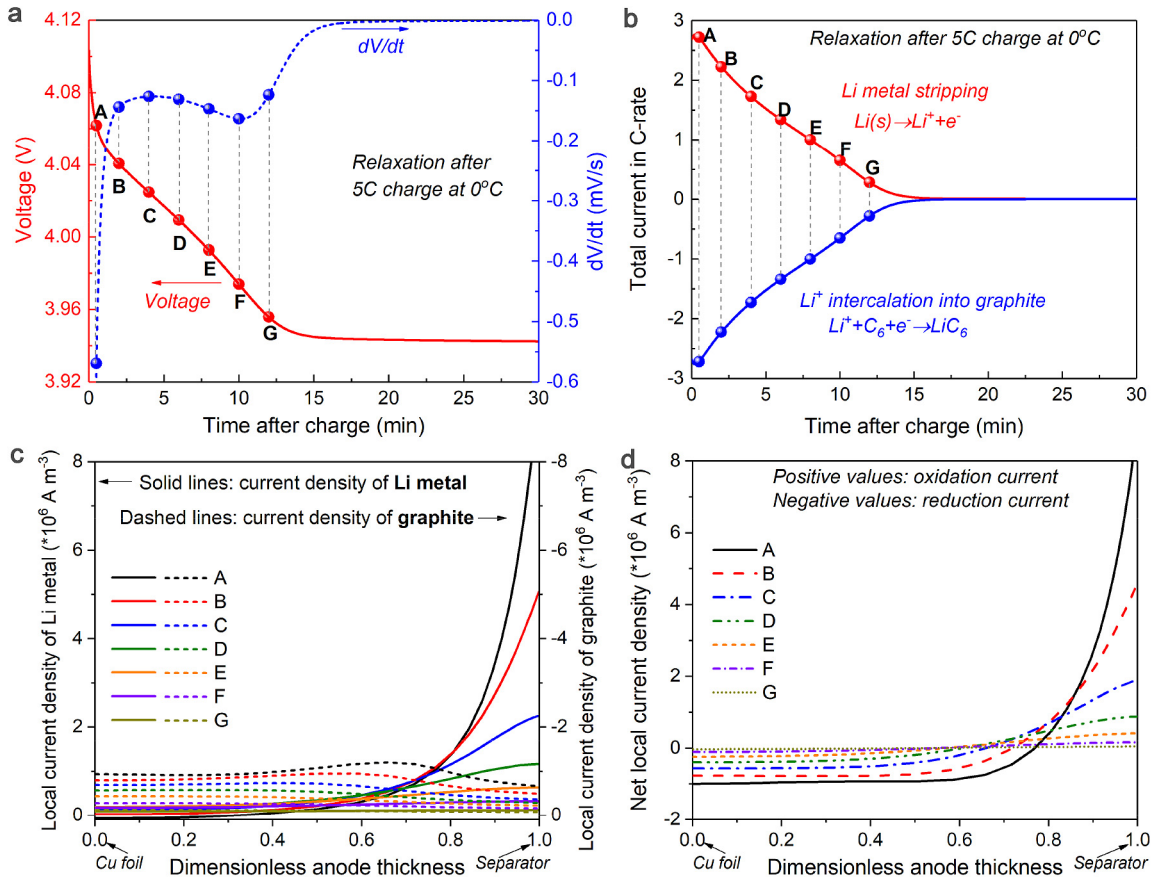

Fig. 3. Local imbalance of stripping and intercalation currents. (a) Selected data points for detailed analysis from the voltage relaxation curves after 5C charge. (b) Overall current of each individual reaction (Li metal stripping and Li^+ intercalation) in the anode during the relaxation process after 5C charge. (c&d) Distributions of (c) local transfer current densities of Li stripping reaction and Li^+ intercalation reaction and (d) local net current density (sum of the current density of the two individual reactions) along the anode thickness at the selected data points.

DI water-based slurry onto 10 μm thick copper foil, whose dry material consisted of graphite (95.4 wt%), Super-C65 (1.0 wt%), SBR (2.2 wt%) and CMC (1.4 wt%). The areal loading of NMC622 is 10.57 mg/cm^2 (1.85 mAh/cm^2) and the areal loading of graphite is 6.678 mg/cm^2 (2.2 mAh/cm^2). The cell consists of 34 anode layers and 33 cathode layers. The nominal capacity of the cell is 9.5Ah and the specific energy is 170 Wh/kg.

Two sets of tests were performed in this study. The first set is to study the voltage plateau during relaxation (open-circuit) after low-temperature charging, and the second is to study the voltage plateau during discharge after charging. In the first sets of tests, the cell was charged at 0 °C ambient from 0% to 80% state of charge (SOC) using the constant current constant voltage (CCCV) protocol, with a constant current ranging from 1C to 5C to a cut-off voltage of 4.2V. Once reaching 80% SOC, the cell was left at open-circuit in 0 °C ambient for 4 h to study the voltage relaxation behavior. Thereafter, the cell was warmed up to 25 °C, charged with CCCV (C/3, 4.2V) protocol to 100% SOC (cut-off current < C/20), discharged at C/3 to 2.7V, and cooled down to 0 °C before performing the next test. In the second set of tests, the cell was charged at 0 °C using CCCV protocol with 5C rate limited by 4.2V until reaching 80% SOC, and discharged immediately after charging at a constant current of either C/3 or 1C to 2.7V.

4. Results & discussion

4.1. Voltage plateau during relaxation

4.1.1. Model validation and analysis of dV/dt peak

Fig. 1a compares model results with experiment data in terms of cell voltage and temperature during charging at 0 °C with different C-rates. The model and experiment results agree reasonably well. The cell was kept at open-circuit after charging to 80% SOC. Cell voltage and differential voltage (dV/dt) during the relaxation process are plotted in Fig. 1c and 1d. In agreement with results in the literature, a voltage plateau appears in the early stage of relaxation, leading to a peak in the dV/dt plot. Comparing modeling results with experiment, we can learn that the present model well captures the shapes of both voltage and differential voltage curves, though with slight discrepancies (e.g. locations of dV/dt peaks). Further, we shall note that the model reasonably predicts the impacts of charge rate on voltage relaxation curve. That is, the increase of charge rate leads to a higher voltage value and a longer duration of the voltage plateau, which can be attributed to the larger amount of Li plated at higher charge rate, as shown in Fig. 1b.

It is proposed in the literature that the dV/dt peak indicates the end of Li stripping [33, 35]. The validity of this assumption is examined here. Fig. 2a shows the evolution of Li metal amount (in capacity) in the relaxation process for cases after charging at different C-rates. The locations of dV/dt peaks in Fig. 1d are marked in this figure by empty symbols. It can be seen that there is still a certain amount of Li metal in the anode when the dV/dt peak is reached, though the amount is low. It is very interesting to note that the remaining Li metal capacity at the dV/dt peak is almost the same for all cases, even though the initial Li metal capacity (after charging) is much higher at higher charge rates. This result indicates that the dV/dt peak corresponds to a point at which the amount of remaining Li metal in the anode falls below a certain critical value. Furthermore, it is worth mentioning that the case of 1C charge at 0 °C has neither a voltage plateau nor a dV/dt peak during relaxation, which can be ascribed to the small amount of Li

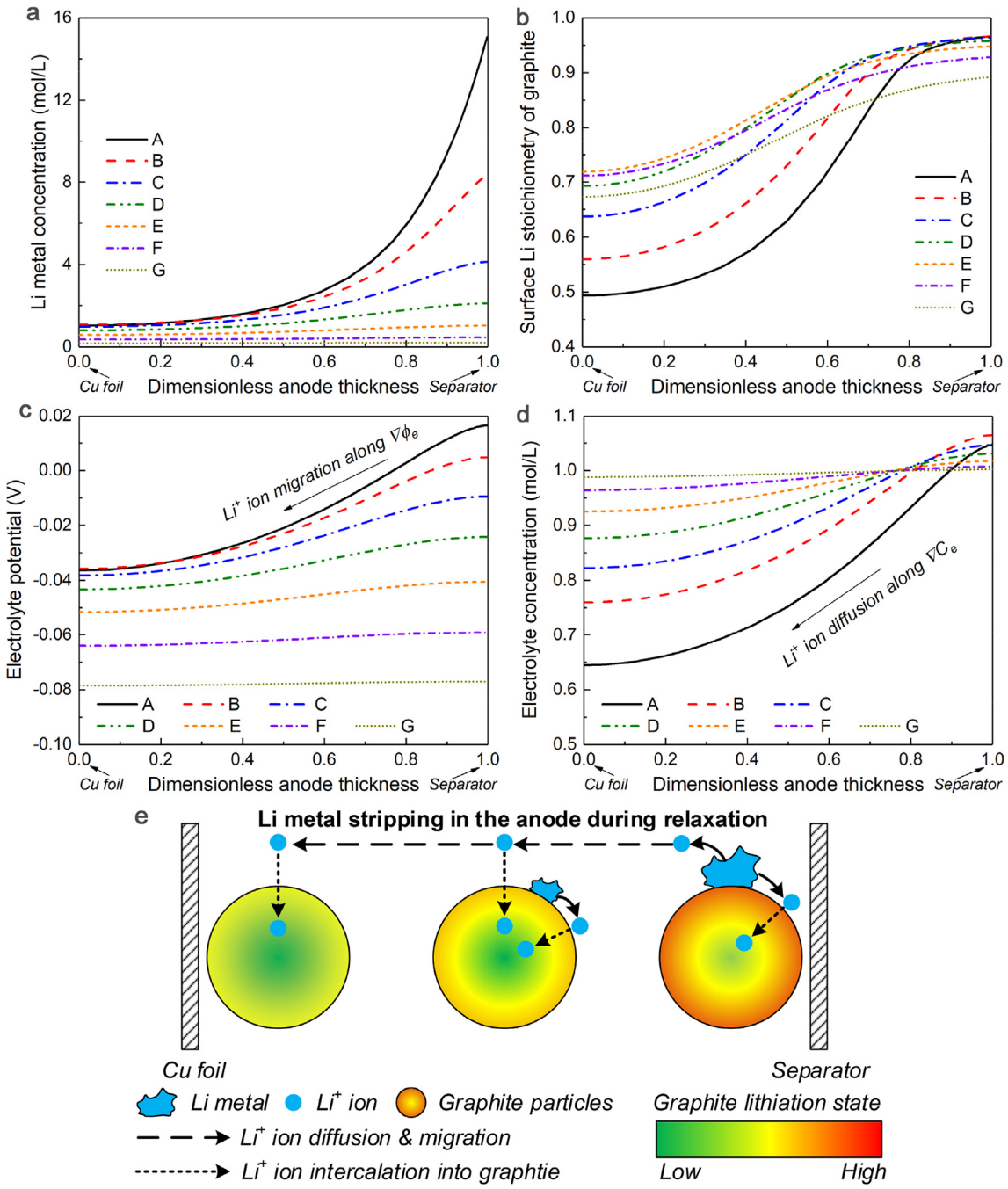

Fig. 4. Internal cell characteristics during relaxation. (a-d) Distributions of (a) Li metal concentration, (b) Li^+ stoichiometry at graphite surfaces, (c) electrolyte potential and (d) electrolyte concentration along the thickness of anode at the selected data points (referring to Fig. 3a) in the relaxation process after 5C charge. (e) Schematic illustration of the internal characteristics of the anode at the beginning of relaxation. After charging, most Li metal is plated near the separator, and the lithiation degree of graphite is also highly non-uniform. The high lithiation degree near the separator restricts the rate capability of Li^+ intercalation. The local rate of Li stripping exceeds the limiting current of Li^+ intercalation near the separator. Li^+ ions that cannot be consumed near the separator move towards the foil along electric field (migration) and concentration gradient (diffusion) and are intercalated into graphite along the path.

plated during charging. Thus, it can be drawn that the voltage plateau and dV/dt peak appear only when Li metal amount exceeds a certain threshold. Even if voltage plateau is not detected, there can still be a small amount of Li plating during charging.

It is also suggested in the literature that the duration of voltage plateau (the time to reach the dV/dt peak) can be used as a metric for assessing the amount of Li plating in different cases. To justify this method, we plot in Fig. 2b the total capacity of Li metal stripped when reaching the dV/dt peak against the time to reach this peak. We can learn that larger amount of Li plating takes a longer time to reach the dV/dt peak. Hence, it can be reasonable to say that longer duration of voltage plateau means larger amount of Li plating. This statement, however, is valid only when comparing cases of the same cell at similar temperatures. As will be discussed in section 4.1.3, the duration of voltage plateau depends highly on the capability of Li^+ intercalation into graphite.

4.1.2. *Internal cell characteristics during voltage relaxation*

In this section, we focus on exploring the internal cell characteristics during the process of voltage relaxation plateau by analyzing the

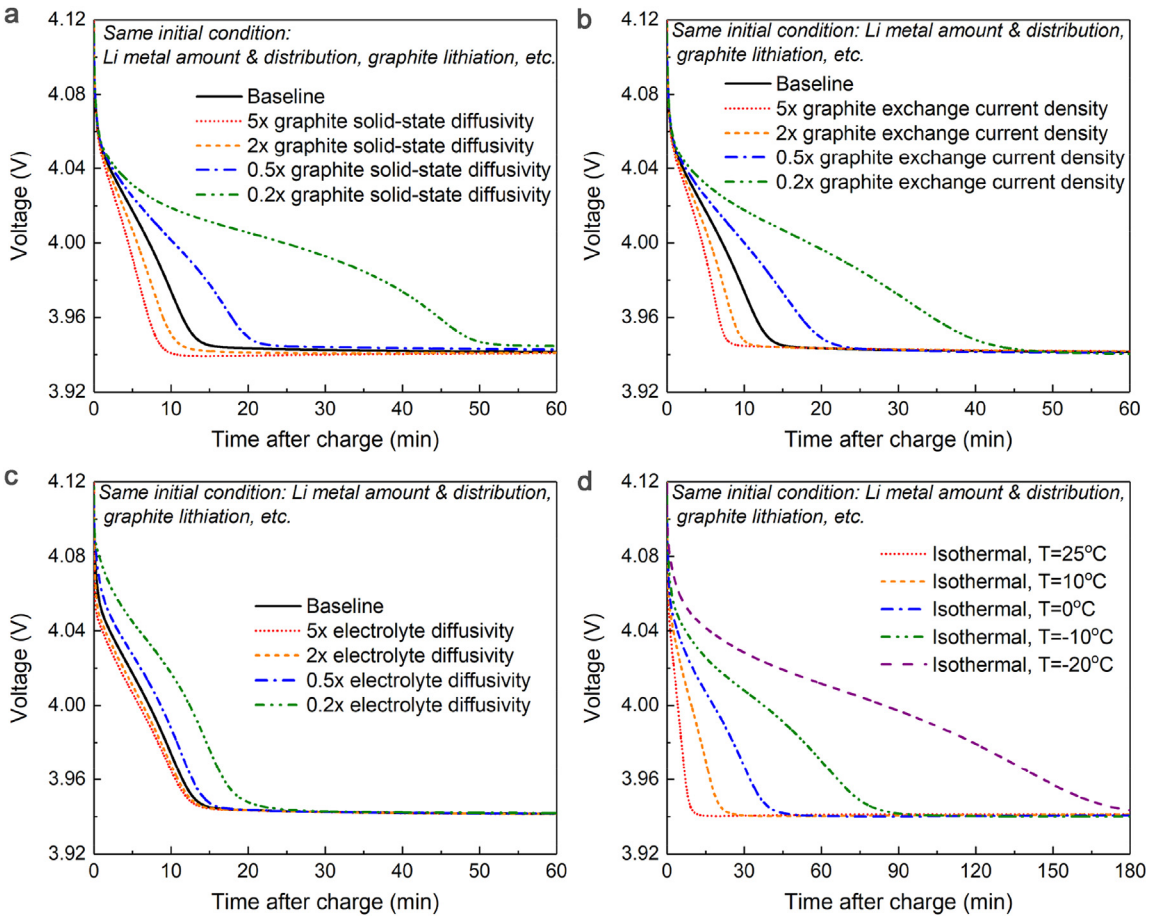

Fig. 5. Key factors affecting voltage relaxation curves. Impacts of (a) solid-state diffusivity of graphite, (b) exchange current density of graphite, (c) electrolyte diffusivity and (d) temperature on the voltage relaxation curves. The initial condition is the same for all cases, which corresponds to the case in Fig. 1 after 5C charge to 80% state of charge. Even with the same initial amount and distribution of Li metal, voltage relaxation curves can be substantially different.

modeling results. Several representative data points from the voltage relaxation curves after the case of 5C charging are selected for detailed analysis, as marked and labeled in Fig. 3a.

During relaxation, two individual reactions occur in the anode: stripping of deposited Li metal and intercalation of Li^+ into graphite. The overall rate of Li stripping is equal to that of intercalation as the cell is at open-circuit. Fig. 3b shows the evolution of overall current of each reaction in the relaxation process. Though the net current is zero, the rate of each reaction is as high as 2.75C at the beginning and drops with time upon relaxation. Fig. 3c presents the distributions of the volumetric (transfer) current density of the two reactions across the thickness of anode at the selected points. It can be seen that the distribution of local Li stripping current density is highly non-uniform, with much higher values near the separator; whereas the rate of Li^+ intercalation is relatively uniform. As such, a very interesting finding here is that the local current density in the anode is not balanced, as shown in Fig. 3d where the distributions of net current density (sum of Li stripping rate and intercalation rate, j_{tot} in Eq. (6)) are given. The anode splits into two regions. The part near the separator has net positive (oxidation) current, generating extra Li^+ ions and electrons. In the meantime, the part near the foil has net negative (reduction) current, indicating additional Li^+ ions and electrons flowing into this region, which are those generated in the region near separator. An interesting question is, why the Li^+ ions near the separator are not completely consumed locally, but travel such a long path to be intercalated in a region far away?

This question can be answered by Fig. 4. After charging, a large amount of Li metal resides in a narrow region near the separator (Fig. 4a), leading to high Li stripping rate in this region (Fig. 3c). In the meantime, the lithiation degree of graphite after charging (Fig. 4b) is also highly non-uniform across the anode. The Li^+ stoichiometry at graphite surface is as high as ~0.95 near the separator while is only ~0.5 near the anode foil at the beginning of discharge. The high surface stoichiometry near the separator can significantly lower the rate capability of Li^+ intercalation in two aspects. First, the exchange current density of graphite drops considerably at high surface stoichiometry, as can be drawn from Eq. (9) (i.e. the exchange current density is proportional to a term $c_{s,i}^{\alpha_{c,gr}}(c_{s,\max}-c_{s,i})^{\alpha_{a,gr}}$). Second, the solid-state diffusivity of graphite also drops with the increase of stoichiometry. As such, the large amount of Li^+ ions generated by stripping reaction near the separator exceed the maximum capability of Li^+ intercalation into graphite. Given the law of charge conservation, all Li^+ ions and electrons generated by the stripping (oxidation) reaction shall be consumed by the intercalation (reduction) reaction. Electric field (Fig. 4c) and electrolyte concentration gradient (Fig. 4d) thus form cross the anode, driving Li^+ ions towards the foil under migration and diffusion.

In summation, the cell characteristics in the early stage of relaxation are illustrated in Fig. 4e. A large amount of Li metal near the separator leads to a high local rate of Li stripping. In the meantime, the rate capability of Li^+ intercalation is restricted near the separator due to the high lithiation degree of graphite. The rate of Li stripping exceeds the locally maximum capability of Li^+ intercalation. Extra Li^+ ions move towards the foil under electric field (migration) and concentration gradient (diffusion), and are consumed along the path. Hence, the anode split into two parts: a local “anode” near the separator which provides Li^+ ions and electrons to a local “cathode” near the foil.

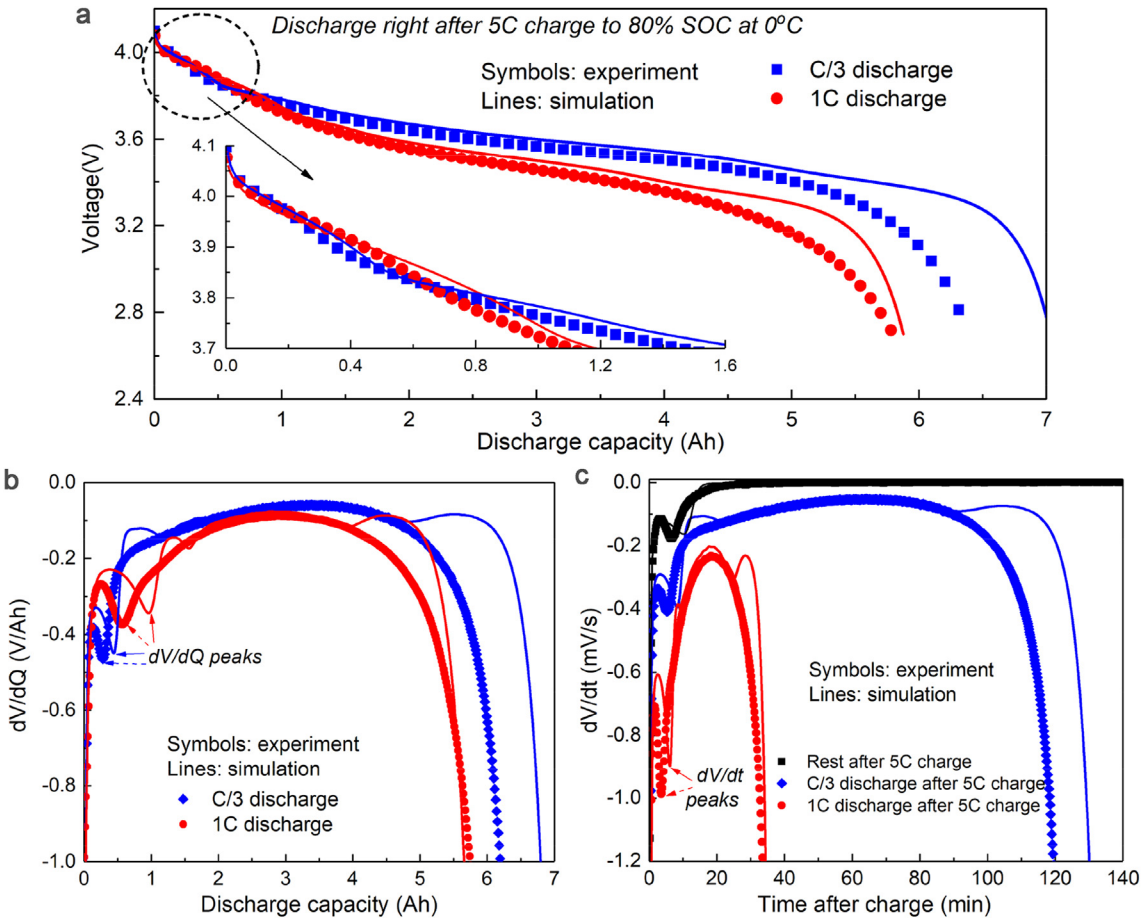

Fig. 6. Discharge voltage plateau and differential voltage curves. (a) Cell voltage during discharge at C/3 or 1C rate after 5C charge to 80% state of charge at 0 °C. The inset is an enlarged view of the beginning of discharge. (b) Differential voltage over capacity (dV/dQ) as a function of discharge capacity in the discharge process. (c) Differential voltage over time (dV/dt) as a function of time for the two discharge cases and the relaxation case after 5C charge (referring to Fig. 3a).

4.1.3. Duration of voltage plateau is dictated by the capability of Li intercalation

It can be drawn from the above discussion that the rate of Li stripping is affected by the capability of Li^+ intercalation into graphite and by the rate of Li^+ diffusion and migration from the separator to the foil. As the voltage relaxation curve depends highly on the rate of Li stripping, we explore in this section the impacts of different parameters on voltage relaxation curves. To perform parametric studies, we chose the cell condition after 5C charge to 80% SOC as the initial condition. That is, all parameters representing internal cell statuses after the 5C charge, such as distributions of Li metal concentration and electrolyte concentration across the cell thickness, distributions of Li^+ stoichiometry in graphite particles, etc., are selected as input parameters for parametric studies.

Fig. 5a and 5b shows the impacts of graphite solid state diffusivity and exchange current density on the voltage relaxation curves. It can be seen that either the exchange current density or solid-state diffusivity of graphite has considerable impacts on the voltage relaxation curves. Even though all cases have the same initial amount and distribution of Li metal, voltage relaxation curves can be substantially different. The reduced capability of Li^+ intercalation, either with reduced solid-state diffusivity or reduced exchange current density, leads to a lower rate of Li stripping (see Fig. S1), and hence to longer duration of voltage plateau. In addition, the diffusivity of electrolyte also affects the voltage relaxation curves, as shown in Fig. 5c. A drop of electrolyte diffusivity reduces the rate of Li^+ ion diffusion from the separator to the foil as discussed above, and accordingly reduces the Li stripping rate (Fig. S1) and increases the duration of voltage plateau. Nevertheless, comparing Fig. 5c with Figs. 5a and 5b we can learn that the impacts of electrolyte property are marginal. Therefore, it can be concluded that the rate of Li stripping is dominated by the rate capability of Li^+ intercalation into graphite. In other words, Li^+ intercalation is the rate-limiting step for Li stripping. Furthermore, as both graphite solid-state diffusivity and exchange current density depend highly on temperature, we further examine the temperature impacts on voltage relaxation in Fig. 5d. All cases in this figure are based on the same initial condition except cell temperature, and we can learn that the voltage plateau is substantially longer at lower temperatures.

It can be learned from Fig. 5 that the voltage relaxation curve can be significantly different even with the same amount of Li plating. The duration of voltage plateau depends on the capability of Li^+ intercalation into graphite. Therefore, the method of using the duration of voltage plateau for comparison of Li plating amount among different tests is reasonable only for tests with the same cell at similar testing temperatures.

4.2. Voltage plateau during discharge

4.2.1. Model validation and interpretation of dV/dQ peaks

The above work focuses on voltage plateau during relaxation. In this section, we investigate another type of voltage plateau reported in the literature, which occurs at the beginning of discharge after charging. Specifically, we focus on internal cell characteristics in this process, and provide a detailed analysis on the interpretation of dV/dQ peak.

Fig. 6a shows the voltage profiles during discharge at two different C-rates (C/3 and 1C) immediately after 5C charge to 80% SOC at 0 °C

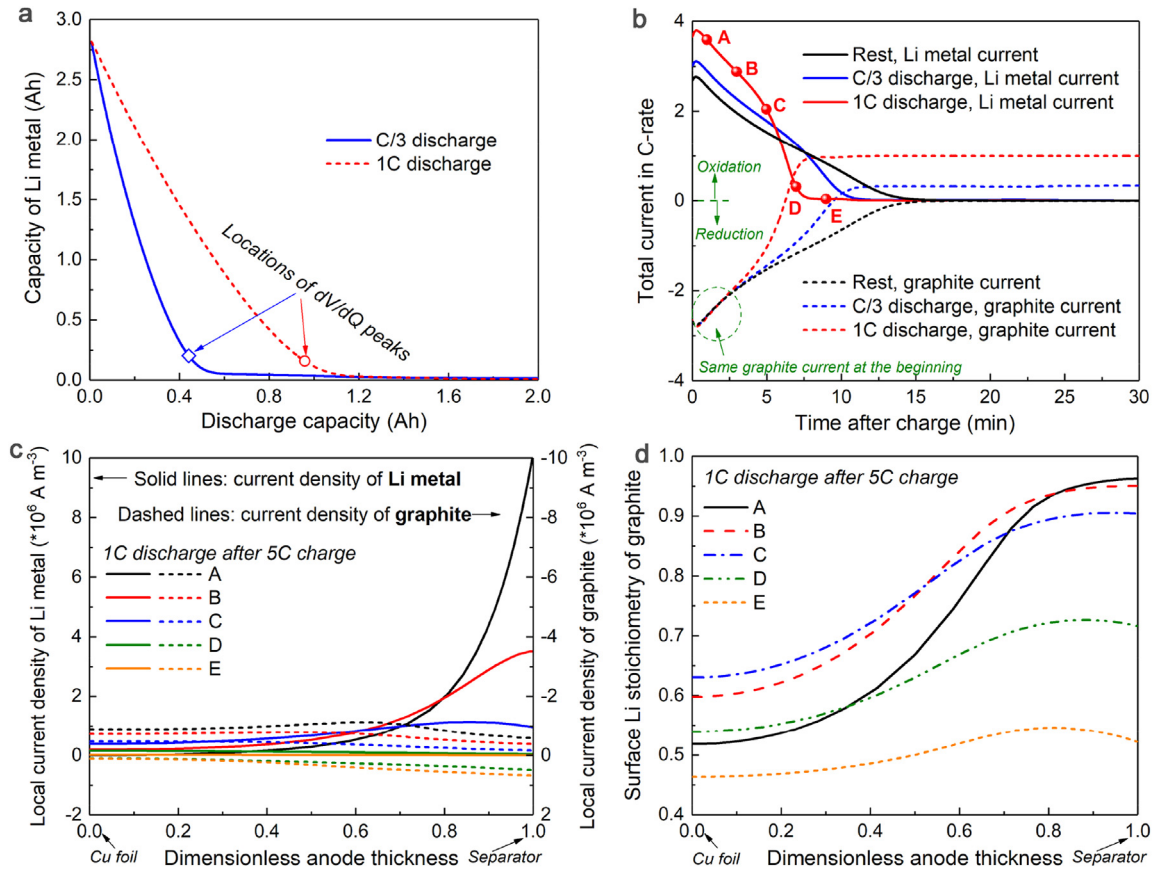

Fig. 7. (a) Remaining capacity of Li metal in the cell vs discharge capacity at two different discharge rates. Empty symbols correspond to the dV/dQ peaks in Fig. 6b. The locations of the dV/dQ peak differ greatly even with the same amount of Li metal at the beginning of discharge. (b) Total rate of Li stripping and Li^+ intercalation/de-intercalation of graphite vs time after charging. Li^+ intercalation occurs at the beginning though the cell is discharging. (c&d) Distributions of (c) local volumetric current densities of Li metal and graphite and (d) Li^+ stoichiometry at graphite surfaces along the thickness of anode at selected data points (referring to Fig. 7b).

ambient. Both modeling and experimental results are plotted, and the inset gives an enlarged view of cell voltage at the beginning of discharge, where we can see clear voltage plateaus in both cases. It can be noted that the present model well captures the feature of discharge voltage plateau.

Fig. 6b plots the derivative of cell voltage over discharge capacity (dV/dQ) of the two cases. In each case, a local dV/dQ peak appears at the beginning of discharge, which agrees with results in the literature. This feature of dV/dQ peak is well predicted by the present model, though the predicted location of the dV/dQ peak is slightly different from experiment. Nevertheless, we shall note that the model is able to capture the same impacts of charge rate on the location of dV/dQ peak. In both the simulations and experiments, the dV/dQ peak appears earlier in the case of C/3 discharge than that of 1C. In the literature, it is proposed that the discharge capacity at the dV/dQ peak equals to the amount of Li deposited during charging and hence can be used for estimating Li plating amount [31]. Clearly, this is not the case in the present study. As shown in Fig. 6b, the two discharge cases are from the same initial condition (5C charge to 80% SOC at 0 °C) and thus should have similar Li plating amount. The discharge capacity at the dV/dQ peak, however, differ greatly in the two cases. Fig. 7a further plots the simulation results of the remaining Li metal capacity in the cell as a function of discharge capacity. The dV/dQ peak is reached at the discharge capacity of 0.4Ah in the C/3 case and 0.95Ah in the 1C case, both of which are significantly lower than the total amount of Li plated during charge (2.8Ah). Hence, it can be drawn that the approach of using discharge capacity at dV/dQ peak for quantification of Li plating would greatly underestimate the actual amount of Li plating.

4.2.2. *Internal cell characteristics during discharge voltage plateau*

The great difference between the discharge capacity at the dV/dQ peak and the total capacity of Li plating is ascribed to the intercalation of Li^+ into graphite which occurs simultaneously with Li stripping. Fig. 7b compares the overall reaction rate of Li metal and graphite in the anode after the 5C charge. The case of relaxation after 5C charge is also added for comparison. We can learn that the increase of discharge rate (from open-circuit to 1C) leads to higher rate of Li stripping. As such, Li metal dissolves faster at higher discharge rate. Plotting dV/dt curves (Fig. 6c) we can see that the dV/dt peak appears earlier at higher discharge rate. It can also be noted from Fig. 7b that Li^+ ions are intercalated into graphite at the beginning, though the cell is discharging. Moreover, it is very interesting to note that the total rate of Li^+ intercalation at the beginning is the same in all cases, despite the difference in discharge rate, which confirms that Li^+ intercalation reaction reaches its limiting current at the beginning. Increasing the output discharge current leads to higher rate of Li stripping to fulfill the external current demand, but does not affect the total rate of Li^+ intercalation at the beginning. Only when Li stripping rate drops significantly would graphite begin to de-intercalate in order to sustain the output current, as can be seen from Fig. 7b.

To further explore the internal cell characteristics in the process of discharge voltage plateau, several representative points are selected from the 1C discharge curve in Fig. 7b for detailed analysis. Fig. 7c shows the distributions of the local current density of Li metal and graphite along the thickness of anode at the selected points. Similar to the case of relaxation (Fig. 3), the distribution of local Li stripping current density is highly non-uniform with extremely high values near

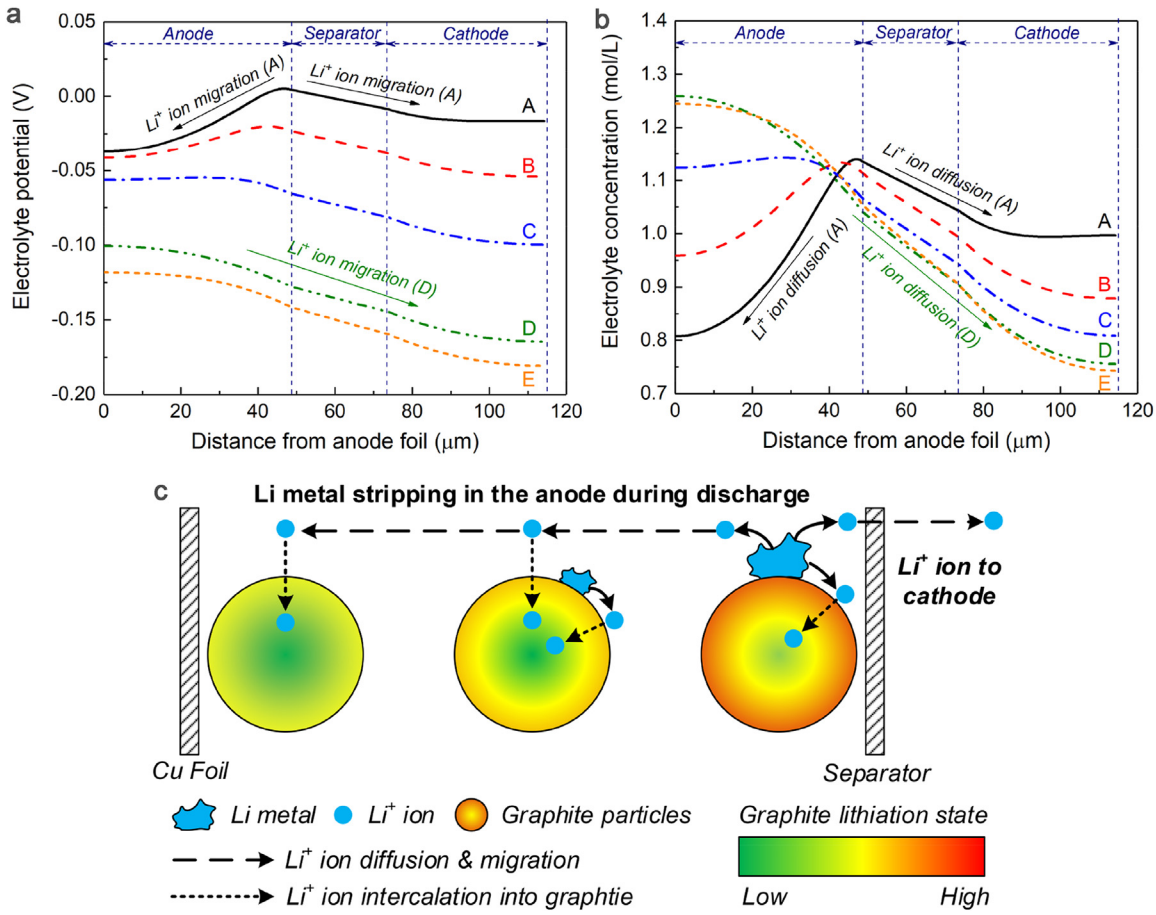

Fig. 8. Internal cell characteristics in the discharge process after charging with Li plating. (a&b) Distributions of (a) electrolyte potential and (b) electrolyte concentration along the thickness of anode at selected data points (A ~ E, referring to Fig. 7b) of 1C discharge after 5C charge at 0 °C. (c) Schematic illustration of the internal cell characteristics in the anode at the beginning of discharge. Most Li metal is plated near the separator. During discharge, the Li^+ ions generated by Li stripping near the separator has three destinations: locally intercalated into graphite, moving to the cathode to deliver output current, and moving towards the anode foil under electric field (migration) and concentration gradient (diffusion) and are intercalated into graphite along the path.

the separator. In the same time, Li^+ intercalation occurs in the anode from point A to C (Fig. 7c). The rate of Li^+ intercalation is restricted by the high surface stoichiometry near the separator (Fig. 7d) as discussed above, and hence the net current density is positive near the separator and negative near the foil, leading to Li^+ ions moving from the separator towards the foil along the electric field (Fig. 8a) and concentration gradient (Fig. 8b) at the beginning of discharge. It can be seen from Fig. 8a and 8b that both the electrolyte potential and electrolyte concentration reach a peak around the anode/separator interface at the beginning of discharge (points A and B). Therefore, the Li^+ ions from stripping reaction near the separator have three destinations: locally intercalated into graphite, moving towards the anode foil by migration and diffusion, and moving towards the cathode to deliver the output current, as illustrated schematically in Fig. 8c.

5. Conclusions

We have presented a Li-ion battery model with incorporation of both Li plating and stripping to gain a fundamental understanding of the voltage plateau behavior associated with stripping of deposited Li metal. Both relaxation plateau and discharge plateau are studied. Special attention is paid to the internal cell characteristics when the voltage plateau occurs, and to key parameters affecting the rate of Li stripping. In addition, the validity of differential voltage analysis for quantification of Li plating is assessed. The main conclusions are summarized below:

a) The duration of voltage plateau depends on the rate of Li stripping, which is significantly affected by the rate capability of Li^+ intercalation into graphite. Parameters like exchange current density of intercalation, solid-state diffusivity of graphite, and temperature can dramatically influence the voltage curves even with the same amount of Li metal. As such, the method of using voltage plateau duration for comparing Li plating amount of different cases is reasonable only when these cases are performed with the same cell at similar testing temperatures.
b) The anode splits into two parts at the beginning of Li stripping. The part of anode near separator has high local current density of Li stripping which exceeds the limiting current density of Li^+ intercalation. Extra Li^+ ions that cannot be consumed locally move towards the anode foil via diffusion and migration and are intercalated into graphite along the path.
c) In the discharge process after charging, Li^+ intercalation still occurs in the anode as long as the Li stripping reaction can sustain the discharge current. As such, the discharge capacity at the dV/dQ peak would underestimate the actual amount of Li plated.

Acknowledgements

Partial financial support by Pennsylvania Department of Environmental Protection (grant # 4100068680-1), Diefenderfer Chair Endowment and DOE CAEBAT Program under award number DE-EE0006425 is gratefully acknowledged.

Appendix A. Supplementary data

Supplementary data related to this article can be found at http://dx.doi.org/10.1016/j.jpowsour.2018.05.073

References

[1] C.Y. Wang, G. Zhang, S. Ge, T. Xu, Y. Ji, X.G. Yang, Y. Leng, Nature 529 (2016) 515–518.
[2] V. Etacheri, R. Marom, R. Elazari, G. Salitra, D. Aurbach, Energy Environ. Sci. 4 (2011) 3243–3262.
[3] H.R. Jiang, Z. Lu, M.C. Wu, F. Ciucci, T.S. Zhao, Nano Energy 23 (2016) 97–104.
[4] C.R. Birkl, M.R. Roberts, E. McTurk, P.G. Bruce, D.A. Howey, J. Power Sources 341 (2017) 373–386.
[5] M. Dubarry, G. Baure, A. Devie, J. Electrochem. Soc. 165 (2018) A773–A783.
[6] R. Xiong, Y. Duan, J. Cao, Q. Yu, Appl. Energy 217 (2018) 153–165.
[7] T. Waldmann, B.I. Hogg, M. Wohlfahrt-Mehrens, J. Power Sources 384 (2018) 107–124.
[8] Z. Li, J. Huang, B. Yann Liaw, V. Metzler, J. Zhang, J. Power Sources 254 (2014) 168–182.
[9] C.R. Birkl, E. McTurk, S. Zekoll, F.H. Richter, M.R. Roberts, P.G. Bruce, D.A. Howey, J. Electrochem. Soc. 164 (2017) A2644–A2653.
[10] D. Anseán, M. Dubarry, A. Devie, B.Y. Liaw, V.M. García, J.C. Viera, M. González, J. Power Sources 356 (2017) 36–46.
[11] P. Keil, A. Jossen, J. Energy Storage 6 (2016) 125–141.
[12] S. Solchenbach, D. Pritzl, E.J.Y. Kong, J. Landesfeind, H.A. Gasteiger, J. Electrochem. Soc. 163 (2016) A2265–A2272.
[13] Y. Zhang, C.Y. Wang, J. Electrochem. Soc. 156 (2009) A527–A535.
[14] Y. Leng, S. Ge, D. Marple, X.G. Yang, C. Bauer, P. Lamp, C.Y. Wang, J. Electrochem. Soc. 164 (2017) A1037–A1049.
[15] S.J. An, J. Li, C. Daniel, S. Kalnaus, D.L. Wood, J. Electrochem. Soc. 164 (2017) A1755–A1764.
[16] N. Ghanbari, T. Waldmann, M. Kasper, P. Axmann, M. Wohlfahrt-Mehrens, ECS Electrochem. Lett. 4 (2015) A100–A102.
[17] Y. Krämer, C. Birkenmaier, J. Feinauer, A. Hintennach, C.L. Bender, M. Meiler, V. Schmidt, R.E. Dinnebier, T. Schleid, Chem. Eur. J 21 (2015) 6062–6065.
[18] J. Wandt, C. Marino, H.A. Gasteiger, P. Jakes, R.-A. Eichel, J. Granwehr, Energy Environ. Sci. 8 (2015) 1358–1367.
[19] J. Wandt, P. Jakes, J. Granwehr, R.-A. Eichel, H.A. Gasteiger, Mater. Today 21 (2018) 231–240.
[20] J. Arai, Y. Okada, T. Sugiyama, M. Izuka, K. Gotoh, K. Takeda, J. Electrochem. Soc. 162 (2015) A952–A958.
[21] H. Ge, T. Aoki, N. Ikeda, S. Suga, T. Isobe, Z. Li, Y. Tabuchi, J. Zhang, J. Electrochem. Soc. 164 (2017) A1050–A1060.
[22] J.C. Burns, D.A. Stevens, J.R. Dahn, J. Electrochem. Soc. 162 (2015) A959–A964.
[23] Q.Q. Liu, R. Petibon, C.Y. Du, J.R. Dahn, J. Electrochem. Soc. 164 (2017) A1173–A1183.
[24] B. Bitzer, A. Gruhle, J. Power Sources 262 (2014) 297–302.
[25] B. Rieger, S.F. Schuster, S.V. Erhard, P.J. Osswald, A. Rheinfeld, C. Willmann, A. Jossen, J. Energy Storage 8 (2016) 1–5.
[26] C. Birkenmaier, B. Bitzer, M. Harzheim, A. Hintennach, T. Schleid, J. Electrochem. Soc. 162 (2015) A2646–A2650.
[27] F. Grimsmann, T. Gerbert, F. Brauchle, A. Gruhle, J. Parisi, M. Knipper, J. Power Sources 365 (2017) 12–16.
[28] V. Zinth, C. von Lüders, M. Hofmann, J. Hattendorff, I. Buchberger, S. Erhard, J. Rebelo-Kornmeier, A. Jossen, R. Gilles, J. Power Sources 271 (2014) 152–159.
[29] R.V. Bugga, M.C. Smart, ECS Trans. 25 (2010) 241–252.
[30] M.C. Smart, B.V. Ratnakumar, J. Electrochem. Soc. 158 (2011) A379–A389.
[31] M. Petzl, M.A. Danzer, J. Power Sources 254 (2014) 80–87.
[32] C. Uhlmann, J. Illig, M. Ender, R. Schuster, E. Ivers-Tiffée, J. Power Sources 279 (2015) 428–438.
[33] S. Schindler, M. Bauer, M. Petzl, M.A. Danzer, J. Power Sources 304 (2016) 170–180.
[34] M. Bauer, B. Rieger, S. Schindler, P. Keil, M. Wachtler, M.A. Danzer, A. Jossen, J. Energy Storage 10 (2017) 1–10.
[35] C. von Lüders, V. Zinth, S.V. Erhard, P.J. Osswald, M. Hofmann, R. Gilles, A. Jossen, J. Power Sources 342 (2017) 17–23.
[36] T. Waldmann, M. Wohlfahrt-Mehrens, Electrochim. Acta 230 (2017) 454–460.
[37] W. Fang, O.J. Kwon, C.Y. Wang, Int. J. Energy Res. 34 (2010) 107–115.
[38] Y. Ji, Y. Zhang, C.Y. Wang, J. Electrochem. Soc. 160 (2013) A636–A649.
[39] X.G. Yang, C. Bauer, C.Y. Wang, J. Power Sources 327 (2016) 414–422.
[40] X.G. Yang, G. Zhang, C.Y. Wang, J. Power Sources 328 (2016) 203–211.
[41] X.G. Yang, T. Liu, C.Y. Wang, J. Power Sources 342 (2017) 598–604.
[42] L. Liu, J. Park, X. Lin, A.M. Sastry, W. Lu, J. Power Sources 268 (2014) 482–490.
[43] L. Liu, P. Guan, C. Liu, J. Electrochem. Soc. 164 (2017) A3163–A3173.
[44] B. Wu, W. Lu, J. Power Sources 360 (2017) 360–372.
[45] P. Arora, M. Doyle, R.E. White, J. Electrochem. Soc. 146 (1999) 3543–3553.
[46] R.D. Perkins, A.V. Randall, X. Zhang, G.L. Plett, J. Power Sources 209 (2012) 318–325.
[47] N. Legrand, B. Knosp, P. Desprez, F. Lapicque, S. Raël, J. Power Sources 245 (2014) 208–216.
[48] X.G. Yang, Y. Leng, G. Zhang, S. Ge, C.Y. Wang, J. Power Sources 360 (2017) 28–40.
[49] S. Hein, A. Latz, Electrochim. Acta 201 (2016) 354–365.
[50] K.H. Chen, K.N. Wood, E. Kazyak, W.S. LePage, A.L. Davis, A.J. Sanchez, N.P. Dasgupta, J. Mater. Chem. A 5 (2017) 11671–11681.
[51] A.F. Chadwick, G. Vardar, S. DeWitt, A.E.S. Sleightholme, C.W. Monroe, D.J. Siegel, K. Thornton, J. Electrochem. Soc. 163 (2016) A1813–A1821.

Nomenclature

a: specific surface area, m^{-1}
c: concentration, mol m^{-3}
c_p: specific heat, J kg^{-1} K^{-1}
D: diffusion coefficient, m^2 s^{-1}
F: Faraday constant, 96487 C mol^{-1}
h: convective heat transfer coefficient, W $m^{-2}K^{-1}$
i_0: exchange current density, A m^{-2}
j: volumetric current density, A m^{-3}
k: kinetic rate constant, m s^{-1}
Q: heat source, W
r: coordinate in the radial direction, m
R: universal gas constant, 8.314 J mol^{-1} K^{-1}
t: time, s
t_+: transference number
T: temperature, K

Greek

α: charge transfer coefficient
σ: electronic conductivity, S m^{-1}
κ: electrolyte ionic conductivity, S m^{-1}
κ_D: diffusional conductivity, A m^{-1}
ϕ: electric potential, V
η: overpotential, V

Subscripts

e: electrolyte
gr: graphite
Li: lithium
s: solid phase, or surface
tot: total